phys. stat. sol. (b) **199**, 81 (1997)

Subject classification: 63.22.+m; 71.35.-y; 78.30.Fs; S7.12; S8.11

Vibrational Resonant Raman Scattering in Spherical Quantum Dots: Exciton Effects

E. Menéndez (a), C. Trallero-Giner[1]) (b), and M. Cardona (b)

(a) Department of Theoretical Physics, Havana University, Vedado 10400, Havana, Cuba

(b) Max-Planck-Institut für Festkörperforschung, Heisenbergstr. 1, D-70569 Stuttgart, Germany

(Received September 9, 1996)

We develope a theoretical model of first order resonant Raman scattering in spherical nanocrystals which includes excitonic effects. Using a matrix diagonalization technique, the exciton wavefunctions and energy states as a function of quantun dot radius are calculated. The Fröhlich interaction between excitons and optical vibrational modes has been considered in the framework of a continuum theory which includes the mechanical and the electrostatic matching boundary conditions at the interface. The Raman cross section and scattering efficiency are calculated for spherical CdS and GaAs nanocrystals. Contrary to the case of uncorrelated electron-hole pairs, strong scattering appears even in the case of infinite barriers. The results obtained for this case are compared with calculations for finite barriers. The selection rules for optical transitions and exciton–lattice interaction are derived for spherical dots in the dipole approximation. Only exciton states and vibrational modes with angular momentum equal to zero are allowed in this approximation.

1. Introduction

During the last decade, intensive effort has been devoted to study the properties of quasi zero-dimensional heterostructures or quantum dots (QDs). Technological improvements have been accompanied by theoretical work aiming at elucidating their properties. Very recently, the first order resonant Raman scattering via Fröhlich interaction has been investigated for spherical nanocrystals [1]. Within the strong-confinement regime and disregarding the exciton contribution, the electronic intermediate states were considered as uncorrelated electron–hole pairs (EHP). The optical vibrational modes (vibrons) were described by a phenomenological approach including the mechanical and electrostatic matching boundary conditions at the interfaces [2]. The coupled modes have a mixture of TO, LO and surface mode components with the concommitant electrostatic potential. For the Raman intensity and in the dipole approximation, an electron–lattice selection rule that only allows transitions involving vibrational modes with quantum number $l_{\rm p} = 0$ was derived. Recently, Krauss et al. [3] measured the optical vibrons of PbS nanocrystals by Raman and far-infrared spectroscopies, confirming the theoretical predictions concerning the influence of electrostatic and mechanical matching boundary conditions on the vibron modes of semiconductor nanocrystals. Since the Coulomb interaction between electrons and holes has been reported to have appreciable influence in the optical properties of the QDs even in the strong confinement regime [4], the uncorrelated EHP model for the forbidden Raman scattering can only be a first approximation. Moreover,

[1]) Also at Department of Theoretical Physics, Havana University, Vedado 10400, Havana, Cuba.

electron–hole correlation should be important in establishing the resonant Raman profile of these novel semiconductor nanostructures.

The present paper is devoted to a model of the first order resonant Raman scattering which takes into account electron–hole correlation effects via Coulomb interaction. Our goal is to describe quantitatively the effect of Coulomb interaction on the electron–hole excitation energies and wavefunctions in order to obtain the resonant Raman scattering amplitude probability for Fröhlich-type interaction in a spherical quantum dot. We show that the Coulomb correlation determines the resonant scattering efficiency in the case of infinite confinement for electrons and holes. In the next section, we develope a nonperturbative approach for obtaining the exciton states in the framework of the envelope function approximation. The electron and hole bands are assumed to be isotropic and parabolic. This is not strictly correct for III–V and II–VI compounds, which have a complex valence band structure, and the effects of band mixing may be significant. Nevertheless, those effects decrease as the dot radius decreases [5] and they can be disregarded here in a first approximation for small quantum dot radii. The expression for the Fröhlich exciton–vibron interaction matrix element is given and exciton and vibron selection rules are derived. In Section 3 we present calculations for the Raman cross sections and Raman profiles for CdS microcrystallites in glass and GaAs dots in an AlAs matrix. Section 4 summarizes the results.

2. Theory

The differential Raman cross section $\partial^2\sigma/\partial\Omega\,\partial\omega_\mathrm{s}$ per unit solid angle $\partial\Omega$ in a volume V is given by [6]

$$\frac{\partial^2\sigma}{\partial\Omega\,\partial\omega_\mathrm{s}} = \frac{V^2\omega_\mathrm{s}^2\eta_\mathrm{l}\eta_\mathrm{s}^3}{8\pi^3c^4\omega_\mathrm{l}}\, W(\omega_\mathrm{s},\,\mathbf{e}_\mathrm{s})\,, \tag{1}$$

where

$$W(\omega_\mathrm{s},\,\mathbf{e}_\mathrm{s}) = \frac{2\pi}{\hbar}\sum_F |M_{FI}(\omega_\mathrm{s},\,\mathbf{e}_\mathrm{s};\,\omega_\mathrm{l},\,\mathbf{e}_\mathrm{l})|^2\,\delta(\hbar\omega_\mathrm{l}-\hbar\omega_\mathrm{s}-\hbar\omega_\mathrm{p})\,, \tag{2}$$

$\eta_\mathrm{l}(\eta_\mathrm{s})$, $\omega_\mathrm{l}(\omega_\mathrm{s})$ and $\mathbf{e}_\mathrm{l}(\mathbf{e}_\mathrm{s})$ are refractive index, the frequency, and the unit vector of the polarization of the incident (scattered) light, respectively, c is the velocity of light in vacuum and M_{FI} the matrix element for scattering of a photon from state $|I(\omega_\mathrm{l},\,\mathbf{e}_\mathrm{l})\rangle$ to state $|F(\omega_\mathrm{s},\,\mathbf{e}_\mathrm{s})\rangle$ with the simultaneous emission of one vibron of frequency ω_p. Neglecting exciton–polariton effects, and taking into account only resonant terms, the matrix element M_{FI} can be written as a function of exciton–radiation $H_{\mathrm{E-R}}$ and exciton–lattice $H_{\mathrm{E-P}}$ interaction Hamiltonians in lowest order perturbation theory as [7, 8]

$$M_{FI} = \sum_{\mu_1,\mu_2}\frac{\langle F|\,H_{\mathrm{E-R}}\,|\mu_2\rangle\,\langle\mu_2|\,H_{\mathrm{E-P}}\,|\mu_1\rangle\,\langle\mu_1|\,H_{\mathrm{E-R}}\,|I\rangle}{(\hbar\omega_\mathrm{s}-E_{\mu_2}+i\Gamma_{\mu_2})\,(\hbar\omega_\mathrm{l}-E_{\mu_1}+i\Gamma_{\mu_1})}\,, \tag{3}$$

where $|\mu_i\rangle$ $(i=1,\,2)$ refers to excitonic intermediate states, with E_{μ_i} and Γ_{μ_i} the corresponding energy and lifetime broadening. From (1) and (2) follows that the Raman scattering $\partial S/\partial\Omega$ efficiency per unit solid angle is given by

$$\frac{\partial S}{\partial\Omega} = \frac{\omega_\mathrm{l}\omega_\mathrm{s}^3}{4\pi^2}\,\frac{\eta_\mathrm{l}\eta_\mathrm{s}^3}{c^4}\,\frac{V}{(\hbar\omega_\mathrm{l})^2}\sum_F |M_{FI}(\omega_\mathrm{l}-\omega_\mathrm{p},\,\mathbf{e}_\mathrm{s};\,\omega_\mathrm{l},\,\mathbf{e}_\mathrm{l})|^2\,, \tag{4}$$

where in the final state we have a scattered photon with frequency $\omega_{\mathrm{s}} = \omega_{\mathrm{l}} - \omega_{\mathrm{p}}$. The exciton-radiation interaction Hamiltonian can be expressed as

$$H_{\mathrm{E-R}} = \sum_{\boldsymbol{\kappa}, e, \mu} \{T_{cv}^{\mu} D_{\mu}^{+} a_{\kappa, e} + T_{cv}^{\mu *} D_{\mu} a_{\boldsymbol{\kappa}, e}\} + \mathrm{H.C.}\,, \tag{5}$$

where $D_{\mu}^{+}(D_{\mu})$ is the creation (annihilation) operator for excitons with quantum number μ and $\alpha_{\boldsymbol{\kappa}, e}$ the annihilation operator of photons with with wavevector $\boldsymbol{\kappa}$. In Eq. (5) T_{cv}^{μ} is the exciton−photon coupling coefficient which for direct allowed transitions between conduction (c) and valence (v) bands in the electric dipole envelope function approximation is [9]

$$T_{cv}^{\mu} = \frac{e}{m_0} \sqrt{\frac{2\pi\hbar}{\omega\eta^2}} \, \frac{e_{\mathrm{l}} \cdot p_{\mathrm{cv}}}{\sqrt{V}} \int \Psi_{\mu}(\mathbf{r}, \mathbf{r}) \, \mathrm{d}^3\mathbf{r} \tag{6}$$

e and m_0 being the free electron charge and mass, respectively, p_{cv} the bulk momentum matrix element between v and c bands, and Ψ_{μ} the exciton envelope wave function in the QD. The exciton−lattice interaction with long-wavelenth optical vibrons has the following form [8]:

$$H_{\mathrm{E-P}} = \sum_{\nu, \mu_1 \nu_2} S_{\mu_2, \mu_1} D_{\mu_2}^{+} D_{\mu_1} (b_{\nu} + b_{-\nu}^{+})\,; \tag{7}$$

where $b_{\nu}(b_{-\nu}^{+})$ is the vibrons annihilation (creation) operator with quantum number ν. The exciton−vibron coupling constant S_{μ_2, μ_1} can be written as

$$S_{\mu_2, \mu_1} = e \int \Psi_{\mu_2}^{*}(\mathbf{r}_{\mathrm{e}}, \mathbf{r}_{\mathrm{h}}) \, [\varphi_F(\mathbf{r}_{\mathrm{e}}) - \varphi_F(\mathbf{r}_{\mathrm{h}})] \, \Psi_{\mu_1}(\mathbf{r}_{\mathrm{e}}, \mathbf{r}_{\mathrm{h}}) \, \mathrm{d}^3\mathbf{r}_{\mathrm{e}} \, \mathrm{d}^3\mathbf{r}_{\mathrm{h}} \tag{8}$$

with $\mathbf{r}_{\mathrm{e}}(\mathbf{r}_{\mathrm{h}})$ being the electron (hole) coordinate. The term φ_F represents the electrostatic potential associated to the optical lattice oscillations in the quantum dot. To describe the interaction between electron and optical lattice vibration we follow the model of [1, 2]. There, the optical vibrational modes of a spherical QD within a macroscopic continuum model which incorporates the elastic and dielectric properties of the constituent materials were obtained. The model requires the coupling between the electrostatic potential and the mechanical displacement vector $\mathbf{u}$ and the matching conditions are derived from the system of four coupled differential equations for $\mathbf{u}$ and φ. For the case of complete confinement it has been shown that the Fröhlich-type electron−vibron coupling $e\varphi_F$ can be written as [1, 2]

$$e\varphi_F = \frac{C_F}{\sqrt{R}} \, \Phi_{n_{\mathrm{p}}, l_{\mathrm{p}}}(r) \, Y_{l_{\mathrm{p}}, m_{\mathrm{p}}}(\vartheta, \varphi)\,; \tag{9}$$

$$C_F = e \sqrt{2\pi\hbar\omega_{\mathrm{L}}(\varepsilon_{\infty}^{-1} - \varepsilon_0^{-1})}\,, \tag{10}$$

where $\Phi_{n_{\mathrm{p}}, l_{\mathrm{p}}}$ with $n_{\mathrm{p}} = 1, 2, \ldots$, $l_{\mathrm{p}} = 0, 1, \ldots$ is the radial part of the electrostatic potential whose explicit form is given in Refs. 1, 10, $Y_{l_{\mathrm{p}}, m_{\mathrm{p}}}(-l_{\mathrm{p}} \le m_{\mathrm{p}} \le l_{\mathrm{p}})$ a spherical harmonic, ω_{L} the bulk phonon frequency, ε_{∞} the high frequency dielectric constant, and ε_0 the static dielectric constant. These modes have both confined and "surface" character and are neither purely longitudinal nor purely transverse.

2.1 Exciton wave function and correlation energy

We consider a spherical QD formed by a pure semiconductor with parabolic bands and an infinite potential barrier at the sphere surface. In the framework of the envelope function approximation the Hamiltonian for the electron–hole pair (EHP) considering the electron–hole correlation $V(\mathbf{r}_\mathrm{e},\, \mathbf{r}_\mathrm{h})$ via Coulomb interaction is given by

$$\hat{H} = \hat{H}_0 + V(\mathbf{r}_\mathrm{e},\, \mathbf{r}_\mathrm{h})\,, \tag{11}$$

where

$$\hat{H}_0 = -\frac{\hbar^2}{2m_\mathrm{e}}\,\nabla_\mathrm{e}^2 - \frac{\hbar^2}{2m_\mathrm{h}}\,\nabla_\mathrm{h}^2 + V_\mathrm{e}(\mathbf{r}_\mathrm{e}) + V_\mathrm{h}(\mathbf{r}_\mathrm{h})\,. \tag{12}$$

If the surface dielectric mismatch is neglected

$$V(\mathbf{r}_\mathrm{e},\, \mathbf{r}_\mathrm{h}) = -\,\frac{e^2}{\varepsilon_0|\mathbf{r}_\mathrm{e} - \mathbf{r}_\mathrm{h}|}\,. \tag{13}$$

In Eqs. (11) to (13) the subscripts e and h refer to electrons and holes, respectively, m_i and V_i (i = e, h) are their effective mass and spatial confinement potential. In our case $V(\mathbf{r})$ vanishes for $r \le R$ and is infinite otherwise. In Ref. [1] the Raman cross section calculation has been performed considering an uncorrelated EHP described by the wave functions

$$\Psi(\mathbf{r}_\mathrm{e},\, \mathbf{r}_\mathrm{h}) = \varphi_{n_\mathrm{e}, l_\mathrm{e}, m_\mathrm{e}}(\mathbf{r}_\mathrm{e})\; \varphi_{n_\mathrm{h}, l_\mathrm{h}, m_\mathrm{h}}(\mathbf{r}_\mathrm{h}) \tag{14}$$

with energy

$$E_{n_\mathrm{e}, l_\mathrm{e}; n_\mathrm{h}, l_\mathrm{h}} = \frac{\hbar^2}{2R^2}\,\left(\frac{(x_{n_\mathrm{e}}^{(l_\mathrm{e})})^2}{m_\mathrm{e}} + \frac{(x_{n_\mathrm{h}}^{(l_\mathrm{h})})^2}{m_\mathrm{h}}\right), \tag{15}$$

where $x_{n_i}^{(l_i)}$ (i =e, h) are solution of the trascendental Eq. (8) of Ref. [1] and the electronic states $\varphi_{n,l,m}(\mathbf{r})$ are described by the wavefunctions

$$\varphi_{n,l,m}(\mathbf{r}) = R_{n,l}(r)\; Y_{l,m}(\vartheta,\, \phi)\,. \tag{16}$$

The radial part of the wave function in the case of finite V_0 band offset is presented in Ref. [1]. For an infinitely high potential barrier the function $R_{n,l}$ becomes the well-known solution of the infinite spherical potential well problem [11]

$$R_{n,l}(r) = \sqrt{\frac{2}{R^3}}\;\frac{j_\mathrm{l}(x_n^{(l)} r/R)}{|j_{l+1}(x_n^{(l)})|}\,. \tag{17}$$

j_l being the spherical Bessel function of the first type, and $x_n^{(l)}$ its n-th node. We treat the electron–hole correlation in the Hamiltonian (11) by a matrix diagonalization technique [4]. This consists in expanding the exciton wave function in a series of eigenfunctions of H_0, the total angular momentum square $\hat{\mathbf{L}}^2$, and its z-component $\hat{L}_z$. Therefore, we search for solutions of (11) of the form

$$\Psi_{N,\,L,\,M}(\mathbf{r}_\mathrm{e},\, \mathbf{r}_\mathrm{h}) = \sum_\alpha \mathbf{C}(\alpha)\; \Phi_\alpha(\mathbf{r}_\mathrm{e},\, \mathbf{r}_\mathrm{h})\,, \tag{18}$$

N, L and M being the quantum numbers corresponding to the exciton energy E, the angular momentum square and its projection on a quantization axis, while α is the set

of quantum numbers n_e, n_h, l_e, l_h of uncorrelated EHP states. The eigenfunctions of the total momentum $\hat{\mathbf{L}}$ are related to the usual one particle wave functions by [12, 13]

$$\boldsymbol{\Phi}_\alpha(\mathbf{r}_\mathrm{e},\,\mathbf{r}_\mathrm{h}) = \sum_{m_\mathrm{e},\,m_\mathrm{h}} (l_\mathrm{e} l_\mathrm{h} m_\mathrm{e} m_\mathrm{h} \,|\, LM)\; \varphi_{n_\mathrm{e},\,l_\mathrm{e},\,m_\mathrm{e}}(\mathbf{r}_\mathrm{e})\; \varphi_{n_\mathrm{h},\,l_\mathrm{h},\,m_\mathrm{h}}(\mathbf{r}_\mathrm{h})\,, \tag{19}$$

$(l_\mathrm{e},\, l_\mathrm{h},\, m_\mathrm{e},\, m_\mathrm{h} \,|\, LM)$ being the Clebsch-Gordan coefficients [12, 13].

To find the coefficients $C(\alpha)$ in Eq. (18) we substitute $\boldsymbol{\Psi}_{N,\,L,\,M}$ in (11), multiply by $\bar{\boldsymbol{\Phi}}_{\alpha'}(\mathbf{r}_\mathrm{e},\,\mathbf{r}_\mathrm{h})$ and integrate over all $\mathbf{r}_\mathrm{e}$, $\mathbf{r}_\mathrm{h}$ space, so that the following system of equations is obtained

$$\sum_\alpha \left[(E_{n_\mathrm{e},\,l_\mathrm{e};\,n_\mathrm{h},\,l_\mathrm{h}} - E)\;\delta_{\alpha',\,\alpha} + V_{\alpha',\,\alpha}\right] C(\alpha) = 0\,. \tag{20}$$

In this representation the matrix elements of the Coulomb interaction are given by [13]

$$V_{\alpha',\,\alpha} = -\,\frac{2E_R a_B}{R}\;\delta_{L',\,L}\delta_{M',\,M} \sum_{k=0}^{\infty} f_k(l_\mathrm{e},\, l_\mathrm{h},\, l'_\mathrm{e},\, l'_\mathrm{h};\, L)\; G_k(n_\mathrm{e},\, n'_\mathrm{e},\, n_\mathrm{h},\, n'_\mathrm{h},\, l_\mathrm{e} l'_\mathrm{e},\, l_\mathrm{h},\, l'_\mathrm{h})\,, \tag{21}$$

where E_R is the exciton Rydberg and a_B the effective Bohr radius. f_k is expressed in terms of the Wigner's 3j and 6j symbols as

$$\begin{aligned} f_k(l_\mathrm{e},\, l_\mathrm{h},\, l'_\mathrm{e},\, l'_\mathrm{h};\, L) = (-1)^{L\,+\,l_\mathrm{e}\,+\,l_\mathrm{h}} \sqrt{(2l_\mathrm{e}+1)\;(2l'_\mathrm{e}+1)\;(2l_\mathrm{h}+1)\;(2l'_\mathrm{h}+1)} \\ \times \begin{pmatrix} k & l_\mathrm{e} & l'_\mathrm{e} \\ 0 & 0 & 0 \end{pmatrix} \begin{pmatrix} k & l_\mathrm{h} & l'_\mathrm{h} \\ 0 & 0 & 0 \end{pmatrix} \begin{Bmatrix} l_\mathrm{e} & \bar{l}_\mathrm{e} & k \\ \bar{l}_\mathrm{h} & l_\mathrm{h} & L \end{Bmatrix}, \end{aligned} \tag{22}$$

$$\begin{aligned} G_k(n_\mathrm{e},\, n'_\mathrm{e},\, n_\mathrm{h},\, n'_\mathrm{h},\, l_\mathrm{e},\, l'_\mathrm{e},\, l_\mathrm{h} l'_\mathrm{h}) = \int_0^\infty \int_0^\infty R_{n_\mathrm{e} l_\mathrm{e}}(r_\mathrm{e})\; R_{n'_\mathrm{e} l'_\mathrm{e}}(r_\mathrm{e})\; R_{n_\mathrm{h} l_\mathrm{h}}(r_\mathrm{h})\; R_{n'_\mathrm{h} l'_\mathrm{h}}(r_\mathrm{h}) \\ \times \frac{r_<^k}{r_>^{k+1}}\; r_\mathrm{e}^2 r_\mathrm{h}^2\; \mathrm{d}r_\mathrm{e}\; \mathrm{d}r_\mathrm{h} \end{aligned} \tag{23}$$

and $r_\le \equiv \min\,(r_\mathrm{e},\, r_\mathrm{h})$, $r_\ge \equiv \max\,(r_\mathrm{e},\, r_\mathrm{h})$. For the case of infinite barriers the coefficients G_k are numbers independent of semiconductor parameters. It should be noticed that the 3j symbols product in f_k is nonzero only if $\max\,(|l_\mathrm{e} - l'_\mathrm{e}|,\; |l_\mathrm{h} - l'_\mathrm{h}|) \le k \le \min\,(|l_\mathrm{e} + l'_\mathrm{e}|,\; |l_\mathrm{h} + l'_\mathrm{h}|)$. Also, the product of 3-j symbols is zero unless $k + l_\mathrm{h} + l'_\mathrm{h}$ and $k + l_\mathrm{e} + l'_\mathrm{e}$ are even numbers. Hence, if $l_\mathrm{e} + l_\mathrm{h}$ and $l'_\mathrm{e} + l'_\mathrm{h}$ are numbers of different parity, the matrix element vanishes and the states with unequal parity remain unmixed. Below we show that the direct allowed optical transitions are those that produce EHP states with exciton angular momentum $L = 0$. Therefore, for the purpose at hand, we only need to evaluate the Clebsch-Gordan coefficients for $L = M = 0$: [12]

$$\langle l_\mathrm{e} l_\mathrm{h} m_\mathrm{e} m_\mathrm{h} \,|\, 00\rangle = (-1)^{l_\mathrm{e}\,-\,m_\mathrm{e}} \delta_{l_\mathrm{e},\,l_\mathrm{h}} \delta_{m_\mathrm{e},\,-m_\mathrm{h}} / \sqrt{2l_\mathrm{e}+1}\,. \tag{24}$$

2.2 Raman scattering intensity

The matrix element $\langle \mu |\, H_{\mathrm{E-R}} \,| I \rangle$ is proportional to the oscillator strength f. Using Eqs. (18) and (19) and the properties of Clebsch-Gordan coefficients (24), we find that

$$f = \int \boldsymbol{\Psi}_{N,\,L,\,M}(\mathbf{r},\,\mathbf{r})\;\mathrm{d}^3\mathbf{r} = \delta_{L,\,0}\delta_{M,\,0} \sum_{\alpha\,:\,(n_\mathrm{e},\,n_\mathrm{h},\,l)} (-1)^l\;\sqrt{2l+1}\; C_{N,\,0,\,0}(\alpha)\; F_0(l,\, n_\mathrm{e},\, n_\mathrm{h})\,, \tag{25}$$

where

$$F_0(l,\, n_\mathrm{e},\, n_\mathrm{h}) = \int_0^\infty R_{n_\mathrm{e},l}(r)\; R_{n_\mathrm{h},l}(r)\; r^2\; \mathrm{d}r\,. \tag{26}$$

The $L = 0$ exciton states are composed of free EHP states with equal orbital quantum numbers ($l_\mathrm{e} = l_\mathrm{h}$); hence, in the above equations we have replaced l_e and l_h by l. In the infinite barrier approach $F_0(l,\, n_\mathrm{e},\, n_\mathrm{h}) = \delta_{n_\mathrm{e},\, n_\mathrm{h}}$. For the exciton–lattice matrix element corresponding to exciton–vibron transitions we can write after substitution of (19) in (8)

$$\begin{aligned} S_{N',\,L',\,M';\,N,\,L,\,M} = {} & \sum_{\alpha,\alpha'} \bar{C}_{\mu'}(\alpha')\; C_\mu(\alpha) \sum_{m_\mathrm{e},\, m_\mathrm{h},\, m'_\mathrm{e},\, m'_\mathrm{h}} (l_\mathrm{e} l_\mathrm{h} m_\mathrm{e} m_\mathrm{h} \mid LM)\; (l'_\mathrm{e} l'_\mathrm{h} m'_\mathrm{e} m'_\mathrm{h} \mid L'M') \\ & \times \frac{C_F}{\sqrt{R}}\; \{\delta_{n'_\mathrm{h},\, n_\mathrm{h}} \delta_{l'_\mathrm{h} l_\mathrm{h}} \langle n'_\mathrm{e} l'_\mathrm{e}|\; \boldsymbol{\Phi}_{n_\mathrm{p},\, l_\mathrm{p}}\; |n_\mathrm{e},\, l_\mathrm{e}\rangle\; \langle Y_{l'_\mathrm{e},\, m'_\mathrm{e}}|\; Y_{l_\mathrm{p},\, m_\mathrm{p}}\; |Y_{l_\mathrm{e},\, m_\mathrm{e}}\rangle \\ & - \delta_{n'_\mathrm{e} n_\mathrm{e}} \delta_{l'_\mathrm{e} l_\mathrm{e}} \langle n'_\mathrm{h},\, l'_\mathrm{h}|\; \boldsymbol{\Phi}_{n_\mathrm{p},\, l_\mathrm{p}}\; |n_\mathrm{h},\, l_\mathrm{h}\rangle\; \langle Y_{l'_\mathrm{h},\, m'_\mathrm{h}}|\; Y_{l_\mathrm{p},\, m_\mathrm{p}}\; |Y_{l_\mathrm{h},\, m_\mathrm{h}}\rangle\}\,. \end{aligned} \tag{27}$$

2.3 Selection rules

In the dipole approximation only $L = 0$ excitonic states are involved in photon absorption or emission processes. Hence, we only evaluate the exciton–lattice interaction matrix elements $\langle N',\, 0,\, 0|\; H_{\mathrm{E-P}}\; |N,\, 0,\, 0\rangle$. From Eq. (27) and the explicit form of $L = M = 0$ Clebsch-Gordan coefficients (24), we find

$$\begin{aligned} S_{N',\,N} = {} & \frac{C_F}{\sqrt{R}} \sum_{n'_\mathrm{e},\, n_\mathrm{e},\, n'_\mathrm{h},\, n_\mathrm{h},\, l} \bar{C}_{N'} C_N\; \frac{1}{2l+1} \\ & \times \{\delta_{n'_\mathrm{h},\, n_\mathrm{h}} \langle n'_\mathrm{e},\, l|\; \boldsymbol{\Phi}_{n_\mathrm{p},\, l_\mathrm{p}}\; |n_\mathrm{e},\, l\rangle - \delta_{n'_\mathrm{e},\, n_\mathrm{e}} \langle n'_\mathrm{h},\, l|\; \boldsymbol{\Phi}_{n_\mathrm{p},\, l_\mathrm{p}}\; |n_\mathrm{h},\, l\rangle\} \sum_{m=-l}^{l} \langle Y_{l,\,m}|\; Y_{l_\mathrm{p},\, m_\mathrm{p}}\; |Y_{l,\,m}\rangle\,. \end{aligned} \tag{28}$$

Using the addition theorem of spherical harmonics [14] we have

$$\begin{aligned} \sum_{m=-l}^{l} \langle Y_{l,\,m}|\; Y_{l_\mathrm{p},\, m_\mathrm{p}}\; |Y_{l,\,m}\rangle &= \int \sum_{m=-l}^{l} |Y_{l,\,m}(\vartheta,\, \varphi)|^2\; Y_{l_\mathrm{p},\, m_\mathrm{p}}(\vartheta,\, \varphi)\; \mathrm{d}\Omega \\ &= \frac{2l+1}{\sqrt{4\pi}}\; \delta_{l_\mathrm{p},\,0} \delta_{m_\mathrm{p},\,0} \end{aligned} \tag{29}$$

and

$$\begin{aligned} S_{N',\,N} = {} & \delta_{l_\mathrm{p},\,0} \delta_{m_\mathrm{p},\,0}\; \frac{C_F}{\sqrt{4\pi R}} \sum_{n'_\mathrm{e},\, n_\mathrm{e},\, n'_\mathrm{h},\, n_\mathrm{h},\, l} \bar{C}_{N'} C_N \\ & \times \{\delta_{n'_\mathrm{h},\, n_\mathrm{h}} \langle n'_\mathrm{e},\, l|\; \boldsymbol{\Phi}_{n_\mathrm{p},\, l_\mathrm{p}}\; |n_\mathrm{e},\, l\rangle - \delta_{n'_\mathrm{e},\, n_\mathrm{e}} \langle n'_\mathrm{h},\, l|\; \boldsymbol{\Phi}_{n_\mathrm{p},\, l_\mathrm{p}}\; |n_\mathrm{h},\, l\rangle\}\,. \end{aligned} \tag{30}$$

Hence, the vibrational modes are restricted to $l_\mathrm{p} = 0$ and, as in the free electron–hole pair model [1], none of the higher order l_p vibrons contribute to the Raman cross section. The Coulomb interaction mixes differently electron states and hole states (because of the different masses). This leads to Raman scattering *even in the case of infinite electron and hole barriers*. Photon wave vector $\boldsymbol{\varkappa} = \mathbf{0}$ create or annihilate EHP's in the

same spatial points $\mathbf{r}_\mathrm{e} = \mathbf{r}_\mathrm{h} = \mathbf{r}$. This leads to correlated EHP's with total angular momentum $L = 0$. Therefore, the quantum number l_p for the participating vibron in the first order Raman process necessarily has to be zero. The following selection rules are thus obtained

$$\begin{array}{lll} \Delta N \neq 0\,, & L = 0\,, & M = 0 \\ \Delta n_\mathrm{p} \neq 0\,, & l_\mathrm{p} = 0\,, & \text{and} \quad m_\mathrm{p} = 0\,. \end{array} \tag{31}$$

In this case the function $\boldsymbol{\Phi}_{n_\mathrm{p},0}$ is reduced to

$$\boldsymbol{\Phi}_{n_\mathrm{p},0} = \frac{\sqrt{R}}{\mu_\mathrm{p}} \left[j_0 \left(\mu_\mathrm{p} \, \frac{r}{R} \right) - j_0 \left(\mu_\mathrm{p} \right) \right], \qquad r \leq R \tag{32}$$

with eigenfrequencies

$$\omega_\mathrm{p}^2 = \omega_\mathrm{L}^2 - \beta_\mathrm{L}^2 \left(\frac{\mu_\mathrm{p}}{R} \right)^2 . \tag{33}$$

The values of μ_p are obtained by solving the equation $\tan\mu = \mu$ and β_L is a phenomenological parameter describing the bulk LO-phonon dispersion.

Finally, the Raman cross section for the Fröhlich interaction contribution in a spherical quantum dot can be written as

$$\frac{\partial^2 \sigma}{\partial \Omega \, \partial \omega_\mathrm{s}} = S_0 \sum_{n_\mathrm{p}} |M_{FI}|^2 \, \frac{\Gamma_\mathrm{p}/\pi}{\left[\hbar\omega_\mathrm{l} - \hbar\omega_\mathrm{s} - \hbar\omega_\mathrm{p}(n_\mathrm{p}, 0) \right]^2 + \Gamma_\mathrm{p}^2} \,, \tag{34}$$

where the delta function in Eq. (2) has been replaced by a Lorentzian in order to take into account the vibron linewidth Γ_p. The coefficient S_0 is equal to

$$S_0 = \left(\frac{e}{m_0} \right)^4 \left(\frac{2P^2 \omega_\mathrm{s}}{3c^2 \omega_\mathrm{l}} \right)^2 \frac{\eta_\mathrm{s}}{\eta_\mathrm{l}} \frac{\hbar C_F^2}{4\pi R} \,, \tag{35}$$

with $P = \langle X| \, P_x \, |S\rangle$ [6],

$$M_{FI} = \sum_{N,\,N'} \frac{f_N \langle N,\, 0|\, h_{\mathrm{E-P}} \, |N',\, 0\rangle \, f_{N'}}{\left(\hbar\omega_\mathrm{s} - E_{N'} + i\Gamma_{N'} \right) \left(\hbar\omega_\mathrm{l} - E_N + i\Gamma_N \right)} \,, \tag{36}$$

and the dimensionless exciton–lattice interaction $h_{\mathrm{E-P}} \left(H_{\mathrm{E-P}} = \dfrac{C_F}{\sqrt{4\pi R}} \, h_{\mathrm{E-P}} \right)$ has been introduced.

As a limiting case, when Coulomb electron–hole correlation is neglected it follows from Eqs. (21) and (28) that in the infinite barrier approach the Fröhlich contribution to the Raman cross section vanishes.

3. Numerical Evaluation and Discussion of the Obtained Results

Equation (20) is solved by a standard numerical method. Taking a finite number N of terms in the sum of (20), the energies are numerically calculated while the corresponding eigenvectors give the coefficients $C(\alpha)$. It should be pointed out that in our matrix diagonalization scheme we have rearranged the basis functions $\boldsymbol{\Phi}_\alpha(\mathbf{r}_\mathrm{e}, \mathbf{r}_\mathrm{h})$, $\alpha : (n_\mathrm{e}, l_\mathrm{e}, m_\mathrm{e}; n_\mathrm{h}, l_\mathrm{h}, m_\mathrm{h})$ by increasing energy: $\boldsymbol{\Phi}_i(\mathbf{r}_\mathrm{e}, \mathbf{r}_\mathrm{h})$, $i = 1, 2, \ldots$. Then, we replace the series in (18) by a sum from $\boldsymbol{\Phi}_1$ to $\boldsymbol{\Phi}_{N_0}$, with L and M fixed. This procedure is

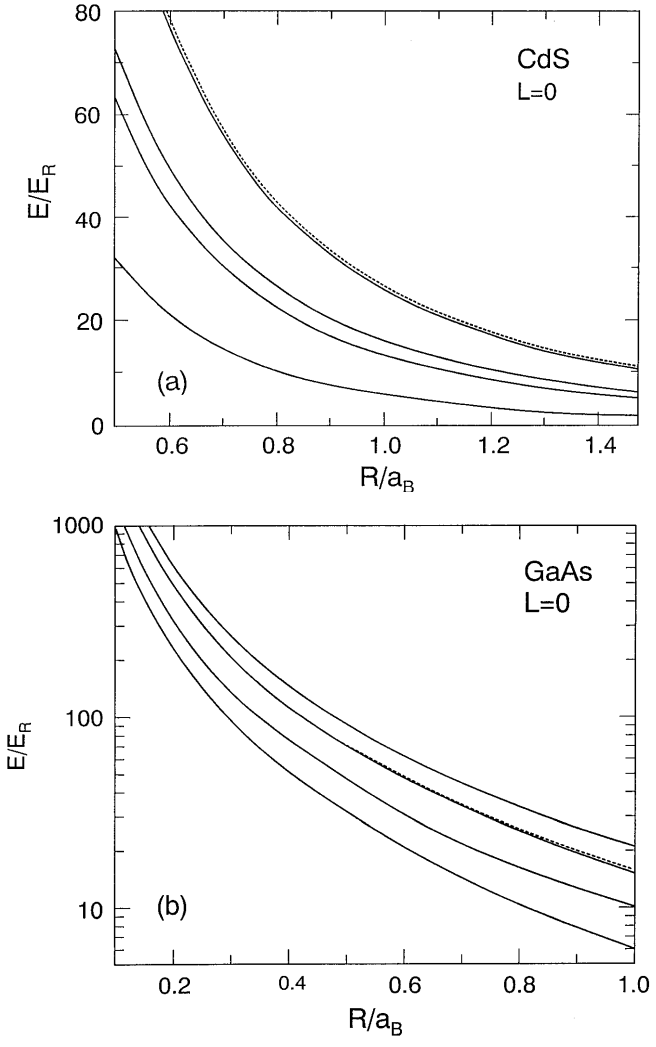

Fig.1. Exciton energy levels solution of equ. (13) for $L = 0$ in units of the exciton Rydberg E_R as a function of the dimensionless radius R/a_B (a_B the effective Bohr radius). a) A CdS sphere embedded in glass; b) GaAs sphere in a matrix of AlAs. Dashed lines represent quasi-degenerate levels

repeated with a larger N_0 until satisfactory stability is obtained for the energy eigenvalues we are interested in. Within this approach we diagonalized matrices much smaller than using "conventional procedures" [4]. In fact, the same results of Ref. [4] are obtained for the low exciton levels in the range $0 < R/a_B < 5$ with 40×40 matrices.

In Fig. 1 we show the $L = 0$ exciton energy of the first levels as a function of QD radius for CdS nanocrystal embedded in glass and for a GaAs dot in an AlAs matrix. The parameters used in our calculations are listed in Table 1. The energy levels and sphere radii are given in units of E_R and a_B, respectively. In this dimensionless scale the low energy level is nearly independent of the ratio of electron and hole masses [15]. In Fig. 1a and 1b quasi-degenerate levels are shown by dashed lines.

In order to take into account the finite band off-set of the barriers for the electrons and holes (essential for Raman scattering to occur) while keeping the mathematical sim-

Table 1
Values of the material parameters used in the numerical calculations

parameter	CdS	glass	GaAs	AlAs
E_g (eV)	2.6 [16]	7 [16]	1.5177 [15]	3.131 [15]
$\omega_{\rm L}$ (cm^{-1})	305 [17]		293.6 [18]	
$\beta_{\rm L}$ (m/s)	5.04×10^3 [1]		3.2×10^3 [18]	
$m_{\rm e}/m_0$	0.18 [17]	1 [1]	0.0665 [15]	0.124 [15]
$m_{\rm h}/m_0$	0.51 [17]	1 [1]	0.45 [15]	0.5 [15]
$V_0^{\rm e}$ (eV)	2.5 [4]		0.968[a]	
$V_0^{\rm h}$ (eV)	1.9 [4]		0.6453[a]	
ε_0	7.8[b]		12.53 [15]	

[a] Calculated assuming band offsets of 60 and 40% of the gap differences for the conduction and valence band, respectively.
[b] Calculated to fit the ground state energy of the bulk exciton given in Ref. [19]

plicity of the infinite confinement approach, we introduce an effective quantum dot radius $R_{\rm ef}$ in such a way that the EHP energy (15) coincides with that for a finite barrier (see Eq. (8) of Ref. [1]). Thus, in the radial part of wave functions (17) and in the uncorrelated EHP energies (15) we replaced R by $R_{\rm ef}$. We fitted the functional dependence of $R_{\rm ef}$ on R and found $R_{\rm ef} = 5.321 + 1.066R - 0.001R^2$, $5\ \text{Å} < R < 35\ \text{Å}$ for CdS microcrystallites embedded in glass and $R_{\rm ef} = 11.259 + 0.971R + 0.0002R^2$, $20\ \text{Å} < R < 120\ \text{Å}$ for GaAs QD in a matrix of AlAs using the barriers of Table I. Note that the vibronic states are characterized by the QD radius (not $R_{\rm ef}$) where the mode amplitude at the surface is zero [1]. We have calculated the one-vibron Raman scattering cross sections and scattering intensities according to Eqs. (1) and (3) for CdS and GaAs quantum dots. According to the selection rules derived in Section 2.3, we have

Table 2
Values of oscillator strength, dimensionless exciton–vibron matrix element $\langle N|\, h_{\rm E-P}^{(n_{\rm p})}\, |N\rangle$ for different $n_{\rm p}$ vibronic modes, and weight coefficient $C(\alpha)$ in the exciton wavefunction (7) contributing to the Raman cross section of Fig. 2

excitonic state	$E_N - E_g$	oscillator strength	$n_{\rm p}$	$d_N^{(n_{\rm p})} = \langle N|\, h_{\rm E-P}^{(n_{\rm p})}\, |N\rangle$	$\lvert C(n_{\rm e}, l; n_{\rm h}, l)\rvert^2$
			$R = 20$ Å		
			1	−0.009	$n_{\rm e}=1,\ n_{\rm h}=1,\ l=1$
1	0.533	0.806	2	−0.0059	0.989
			3	−0.00045	
			$R_{\rm ef} = 26.1$ Å		
			1	−0.012	$n_{\rm e}=1,\ n_{\rm h}=1,\ l=1$
1	0.278	0.749	2	−0.00161	0.98
			3	−0.00018	
			1	−0.0196	$n_{\rm e}=1,\ n_{\rm h}=2,\ l=0$
2	0.605	0.0168	2	−0.074	0.97
			3	−0.003	
			1	−0.00015	$n_{\rm e}=1,\ n_{\rm h}=1,\ l=1$
3	0.710	2.695	2	−0.00149	0.958
			3	−0.00009	

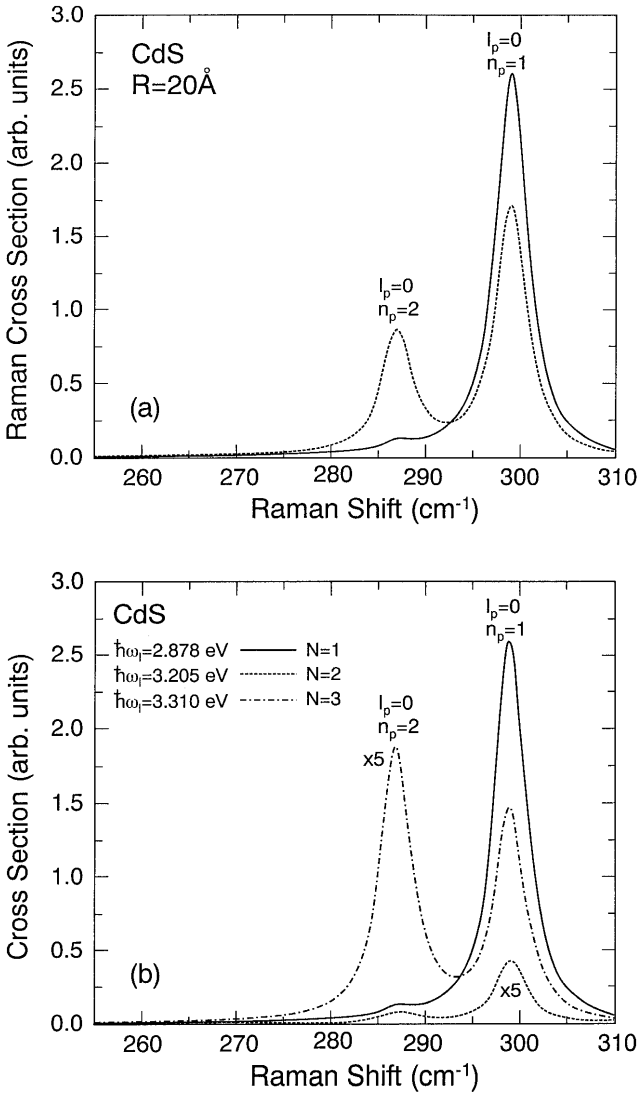

Fig. 2. a) Raman cross section vs. Raman shift for a 20 Å radius CdS sphere embedded in glass at a laser energy in resonance with the $N = 1$ exciton state. Solid line: modeling the finite potential band offset (see text), dashed line: infinite potential barrier. b) Raman spectra at different laser energies $\hbar\omega_l$. The two peaks correspond to $l_p = 0$ vibrons ($n_p = 1$ and $n_p = 2$)

summed in the matrix element M_{FI} of Eq. (3), the first 20 excitonic levels with $L = 0$ for different n_p vibronic modes and $l_p = 0$. A lifetime broadening of 5 meV for all exciton transitions involved and a vibron half width of 2 cm^{-1} were used in the calculation. The $l_p = 0$ vibronic frequencies, of a purely longitudinal character, were obtained with Eq. (33) using the parameters given in Table 1.

In Fig. 2 we show the Raman cross section for a CdS microcrystallite of 20 Å radius as a function of the Raman shift for laser energies on incoming resonance with different

exciton states. The spectrum for $\hbar\omega_l = 3.133$ eV corresponds to an incoming resonance with the lowest energy state assuming completely confined excitons (dashed lines in Fig. 2a). There are contributions due to the $l_p = 0$, $n_p = 1$ mode at 299 cm^{-1} and one more peak at 287 cm^{-1} due to $n_p = 2$ modes.

Modeling the finite potential barrier of the microcrystallite electrons and holes as explained above, we find an effective confinement radius of 26.1 Å for the EHP energy (15) and basis wave functions (17). The solid line in Fig. 2a corresponds to the Raman cross section calculated using $R = 26.1$ Å. The laser energy is in resonance with the corresponding $N = 1$ ground state, i.e. $\hbar\omega_l = 2.878$ eV. Firstly, we note that the $n_p = 1$ vibron is stronger in the case of "finite" confinement. Second, in the infinite barrier case the peak associated to the $n_p = 2$ vibron is enhanced to be of the same order as $n_p = 1$ vibron. In order to understand these feature we report in Table 2 the values of oscillator strength and dimensionless $\langle N|\, h_{E-P}^{(n_p)}\, |N\rangle$ exciton–vibron matrix elements for several n_p vibron modes when the wavefunctions (17) are taken either with $R = 20$ Å or with $R = R_{ef} = 26.1$ Å. The principal contribution to the $N = 1$ matrix element comes from the $n_e = n_h = 1$ and $l = 1$ EHP states. Comparing the absolute values of the exciton–lattice matrix elements in Table 2 we conclude that $|d_1^{(1)}|$ for R_{ef} is 33% higher than that with $R = 20$ Å. Similar analysis can be done for $l_p = 0$ $n_p = 2$ mode, thus explaining the relative intensities respect to $n_p = 1$ ($d_1^{(2)}/d_1^{(1)} = 0.13$ using R_{ef} and $d_1^{(2)}/d_1^{(1)} = 0.65$ evaluated for the QD radius). The electron–hole *decompensation* is greater for the *effective quantum dot* which simulates the finite barrier potential.

In Fig. 2b we show the Raman cross section for the incoming resonances with the $N = 1$, 2 and 3 exciton levels. The latter two spectra have been multiplied by a factor of 5. The spectrum for $\hbar\omega_l = 3.205$ eV ($N = 2$) is much weaker because the exciton state $|N = 2, 0, 0\rangle$ is mostly composed of the pure electron and hole states with $n_e = 1$,

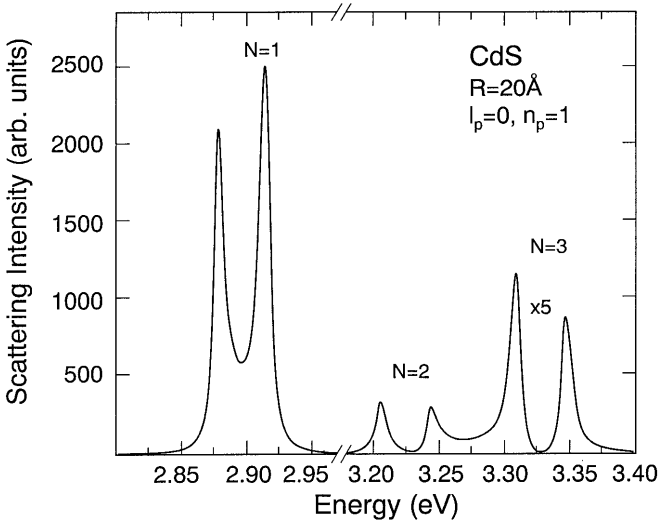

Fig. 3. Raman intensity as a function of laser energy for the $l_p = 0$, $n_p = 1$ mode of a 20 Å radius CdS sphere embedded in glass. The different exciton contributions are shown in the figure ($N = 1$, 2 and 3 excitonic states)

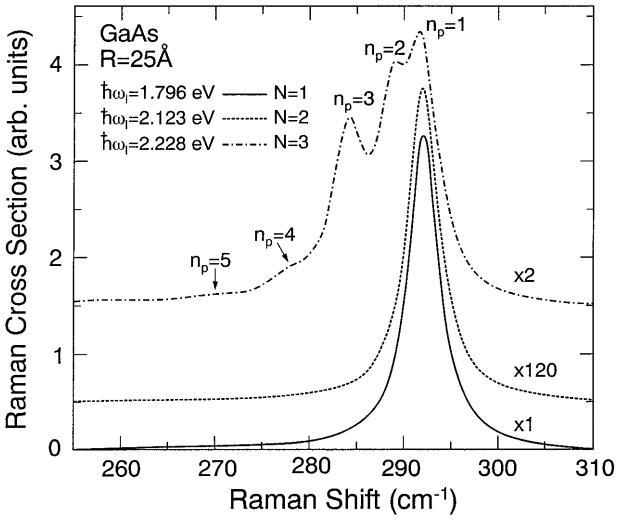

Fig. 4. Raman spectra of a 25 Å radius GaAs sphere in a matrix of AlAs at different laser energies. Solid line: $\hbar\omega_{\rm l}$ in resonance with $N = 1$ excitonic state, dashed line: $\hbar\omega_{\rm l}$ in resonance with $N = 2$ state (multiplied by a factor of 120) and dashed-dotted line: $\hbar\omega_{\rm l}$ in resonance with $N = 3$ excitonic level (multiplied by a factor of 2)

$l_{\rm e} = 0$, $n_{\rm h} = 2$, $l_{\rm h} = 0$ and its optical strength is about 2% that of the first state. On the other hand, the resonance with the $N = 3$ level presents an optical strength 3.6 times larger than that of the first level, nevertheless, the matrix element $\langle 3,\, 0,\, 0|\, H_{\rm E-P}\, |3,\, 0,\, 0\rangle$ is quite small, and the relative intensities of the $n_{\rm p} = 1,\, 2$ vibron peaks must be determined by other virtual transitions.

Fig. 3 displays the integrated Raman intensity obtained according to Eq. (4) for the $l_{\rm p} = 0$, $n_{\rm p} = 1$ mode. The peaks corresponds to the incoming and outgoing resonances with the first, second and third levels. To the right of the breakpoint, the Raman intensity has been also multiplied by 5. The ground state exciton presents an outgoing resonance stronger than the incoming one, while for the excited states $N = 2$ and 3 the opposite is observed. This can be explained by interference effects with other virtual exciton transitions occurring in the respective resonance regions.

The Raman spectra for a GaAs dot of $R = 25$ Å in a AlAs matrix are shown in Fig. 4. The calculated effective radius is equal to 35.5 Å and laser energies are chosen in incoming resonances with the $N = 1,\ 2$ and 3 exciton states. The $\hbar\omega_{\rm l} = 2.123$ eV and $\hbar\omega_{\rm l} = 2.228$ eV spectra have been multiplied by 120 and 2 and shifted 0.5 and 1.5 units

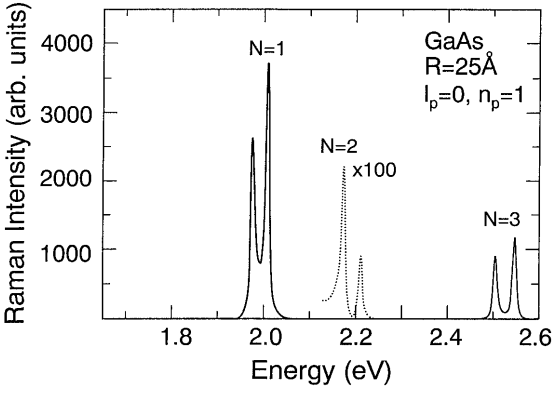

Fig. 5. Raman profile for the $l_{\rm p} = 0$, $n_{\rm p} = 1$ vibron in a 25 Å radius GaAs sphere in a matrix of AlAs. The different exciton contributions are shown in the figure ($N = 1$, 2, and 3 excitonic states). The $N = 2$ level contribution has been multiplied by a factor of 100

upward, respectively. The resonance with $N = 2$ has a smaller cross section due to the small optical oscillator strength. Beside the principal structure at 292 cm^{-1} ($n_p = 1$) the $\hbar\omega_l = 2.228$ eV spectra clearly shows two more peaks at 289 cm^{-1} ($n_p = 2$) and 284 cm^{-1} ($n_p = 3$) and small shoulders at 278 cm^{-1} and 269 cm^{-1} due to $n_p = 4$, 5, respectively. The matrix element M_{FI} for $N = 3$ with $n_p = 1$ intrasubband transition is nearly 35% of that for the $N = 1$, $n_p = 1$ transition. Moreover, the $N = 3$ exciton is about 10 meV below (see Fig. 1) $N = 4$ counterpart and this quasi degeneracy in energy implies an additional increase of the Raman cross section.

In Fig. 5 the integrated Raman intensity for the $n_p = 1$ vibrons in the GaAs nanocrystal of 25 Å radius is presented. The resonances for the $N = 1$ and 3 levels are clearly seen where the outgoing peaks, in both cases, are stronger than the incoming resonances. The structure around the $N = 2$ exciton is very weak (a factor 100 times smaller) reflecting the weak oscillator strength and exciton–lattice matrix element.

4. Conclusions

We have calculated the first order Raman cross section and resonance profile for optical vibrons in semiconductor quantum dots and microcrystals induced by Fröhlich interaction including the electron–hole correlation in the envelope function approximation. We have considered the exciton–vibron Fröhlich-type Hamiltonian within a continuum model for the vibron which incorporates the elastic and dielectric properties of the dot and the surrounding medium. In the dipole approximation and using a one-band effective mass model for the c and v bands, the $L = 0$ and $l_p = 0$ selection rules for the exciton–lattice transitions are obtained for spherical QD. We present the calculated energy of the allowed $L = 0$ excitonic states as a function of quantum dot radius for GaAs and CdS. The finite band offset for electrons and holes has been modeled by introducing an effective dot that corrects the EHP energy in an infinite potential. The finite band offset has a profound influence on the Raman cross sections. The main characteristic of the Raman profile is that the outgoing peak for the $N = 1$ lower exciton energy is higher than for the incoming one. This follows from the zero-dimensional character of excitons in small radius QDs (non interference between different levels). The excited states may present stronger intensity peaks at incoming or outgoing resonances depending on the QD radius, exciton oscillator strength and exciton–vibron matrix element.

Acknowledgements One of us (C.T.-G.) acknowledges the hospitality of Max-Planck-Institut fur Festkörperforschung, Stuttgart, where part of this work was performed. We are grateful to V. I. Belitsky for a critical reading of the manuscript.

References

[1] M. P. Chamberlain, C. Trallero-Giner, and M. Cardona, Phys. Rev B **51**, 1680 (1995).
[2] E. Roca, C. Trallero-Giner, and M. Cardona, Phys. Rev. B **49**, 13704 (1994).
[3] T. D. Krauss, F. W. Wise, and D. B. Turner, Phys. Rev. Letters **76**, 1376 (1996).
[4] Y. Z. Hu, M. Lindberg, and S. W. Koch, Phys. Rev. B **42**, 1713 (1990).
[5] P. C. Sercel and K. J. Vahala, Phys. Rev. B **42**, 3690 (1990).
[6] M. Cardona, in: Light Scattering in Solids II, Ed. M. Cardona and G. Güntherodt, Topics in Applied Physics, Vol. 50, Springer, Heidelberg 1982 (p. 19).
[7] R. Loudon, Proc. Royal Soc. London Ser. A **275**, 219 (1963).

[8] A. K. Ganguly and J. L. Birman, Phys. Rev. **162**, 806 (1967).
[9] R. J. Elliot, Phys. Rev. **108**, 1384 (1957).
[10] C. Trallero-Giner and F. Comas, Phil. Mag. **70**, 583 (1994).
[11] Al. L. Efros and A. L. Efros, Fiz. Tekh. Poluprov. **16**, 1209 (1982); Soviet Phys. – Semicond. **16**, 772 (1982).
[12] A. S. Davydov, Quantum Mechanics, Pergamon Press, Oxford 1976.
[13] D. M. Brink and G. R. Satcher, Angular Momentum, 2nd ed., Oxford Librery of Sciences, Clarendon Press, Oxford 1968 (p. 102).
[14] J. D. Jackson, Classical Electrodinamics, John Wiley, New York 1962.
[15] Y. Kayanuma and H. Momiji, Phys. Rev. B **41**, 1026 (1990).
[16] A. F. Ekimov, Phys. Scripta **T39**, 217 (1991).
[17] A. P. Alivisatos, R. D. Harris, P. J. Carol, M. L. Steigerwald, and L. E. Brus, J. Chem. Phys. **90**, 3463 (1989).
[18] F. Comas, R. Perez-Alvarez, C. Trallero-Giner, and M. Cardona, Superlatt. Microstruct. **14**, 95 (1993).
[19] U. Woggon and S. V. Gaponenko, phys. stat. sol. (b) **189**, 285 (1995).